ACS OMEGA

http://pubs.acs.org/journal/acsodf

Article

Effect of Indium Addition on the Low-Temperature Selective Catalytic Reduction of NO_x by NH_3 over $MnCeO_x$ Catalysts: The Promotion Effect and Mechanism

Changze Yang, Haixia Li,* Anchao Zhang, Zhijun Sun, Xinmin Zhang, Shuaibo Zhang, Leying Jin, and Zhiheng Song

Cite This: *ACS Omega* 2022, 7, 6381−6392

Read Online

ACCESS | Metrics & More | Article Recommendations

ABSTRACT: A $MnCeInO_x$ catalyst was prepared by a coprecipitation method for denitrification of NH_3-SCR (selective catalytic reduction). The catalysts were characterized by Fourier transform infrared spectroscopy (FTIR), X-ray diffractometry, scanning electron microscopy, X-ray photoelectron spectroscopy, Brunauer−Emmett−Teller analysis, H_2 temperature-programmed reduction, and NH_3 temperature-programmed desorption. The NH_3-SCR activity and H_2O and SO_2 resistance of the catalysts were evaluated. The test results showed that the SCR and water resistance and sulfur resistance were good in the range of 125−225 °C. The calcination temperature of the $Mn_6Ce_{0.3}In_{0.7}O_x$ catalyst preparation was studied. The crystallization of the $Mn_6Ce_{0.3}In_{0.7}O_x$ catalyst was poor when calcined at 300 °C; however, the crystallization is excessive at a 500 °C calcination temperature. The influence of space velocity on the performance of the catalyst is great at 100−225 °C. FTIR test results showed that indium distribution on the surface of the catalyst reduced the content of sulfate on the surface, protected the acidic site of MnCe, and improved the sulfur resistance of the catalyst. The excellent performance of the $Mn_6Ce_{0.3}In_{0.7}O_x$ catalyst may be due to its high content of Mn^{4+}, surface adsorbed oxygen species, high specific surface area, redox sites and acid sites on the surface, high turnover frequency, and low apparent activation energy.

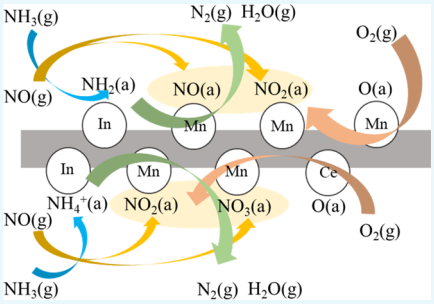

HIGHLIGHTS

- A novel NH_3-SCR catalyst was developed by doping indium into $MnCeO_x$.
- The $MnCeInO_x$ catalyst showed >90% conversion of NO_x at 125−225 °C.
- The resistance to H_2O and SO_2 of the $Mn_6Ce_{0.3}In_{0.7}O_x$ catalyst was enhanced significantly.
- The mechanism of catalysis of NH_3-SCR of the novel catalyst was analyzed.
- The doping of indium improved the TOF value of the catalyst and reduced the apparent activation energy of the catalyst.

1. INTRODUCTION

NO_x is a harmful pollutant produced by fossil fuels mainly from industrial processes and residential life. The natural degradation way is to combine it with water to produce nitric acid into the earth with rain. A large amount of nitric acid combined with rain will form acid rain, and gaseous NO_x will form photochemical smog, which has a great impact on human health and ecological balance.[1] In recent years, the government had higher and higher requirements for NO_x emission standards of enterprises.[2] Many denitrification technologies have been developed to meet the standards.[3−5] At present, the vanadium catalyst (V_2O_5-WO_3/TiO_2) is widely used in industry. Due to its strict high-temperature operating window (290−400 °C) and toxic pollution of vanadium sublimation at high temperatures, the working environment of the catalyst has many restrictions.[6,7] With the improvement of waste heat utilization technology of flue gas in power plants, the requirement of flue gas denitration for catalyst temperature is higher and higher. Therefore, the development of a low-temperature denitration catalyst with high efficiency is very promising.[8,9] NH_3-SCR (selective catalytic reduction) is an approach for effective NO_x reduction.[10] Therefore, it is very promising to develop catalysts suitable for low-temperature NH_3-SCR technology instead of high-temperature active catalysts.

Among all the studied metals, MnO_x is widely studied for its excellent low-temperature catalytic activity, but it cannot be applied in practice due to its poor water and sulfur resistance.[11]

Received: December 10, 2021
Accepted: January 24, 2022
Published: February 8, 2022

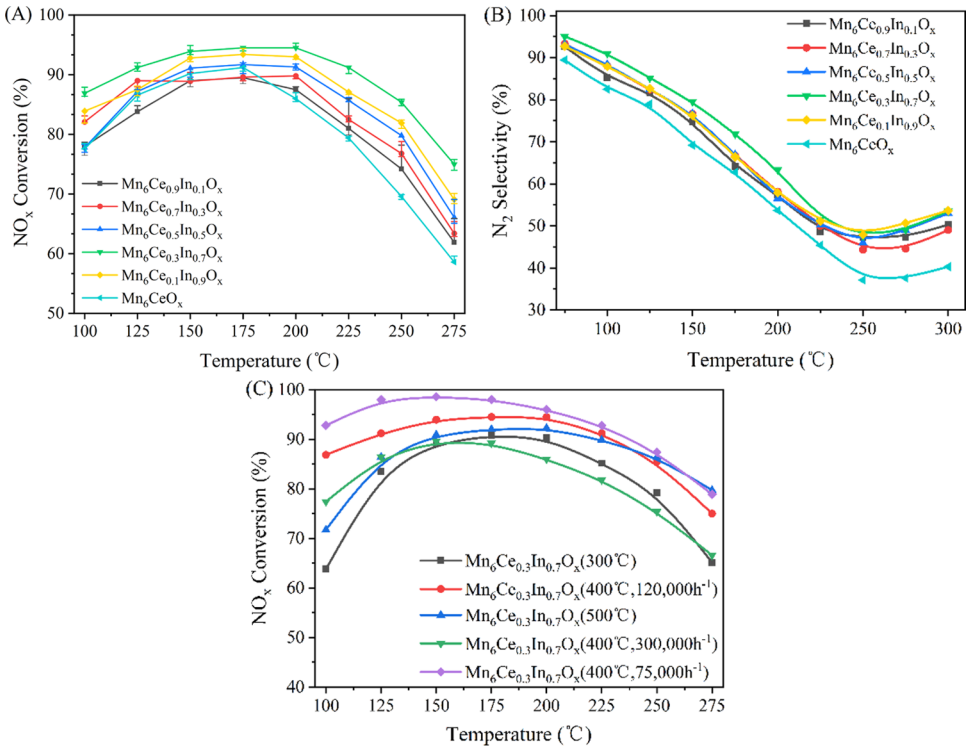

Figure 1. (A) NO_x conversion. (B) N_2 selectivity. Reaction conditions: 500 ppm NH_3, 500 ppm NO, 5 vol % O_2, and balance N_2, with a GHSV of 120,000 h^{-1}. (C) Different temperatures and GHSVs over different catalysts.

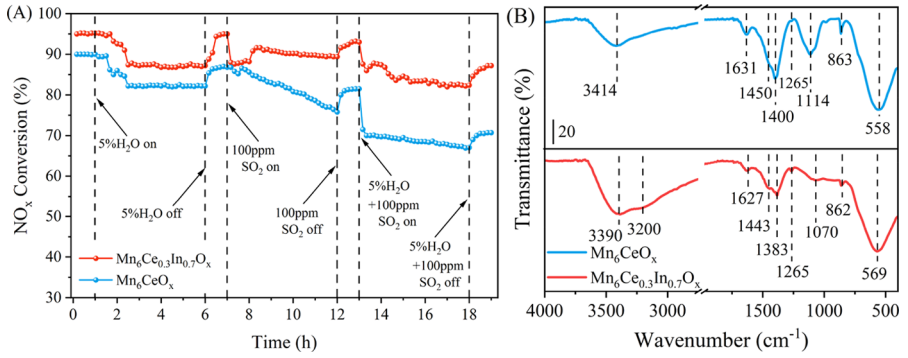

Figure 2. (A) Water and sulfur resistance of $Mn_6Ce_{0.3}In_{0.7}O_x$ and Mn_6CeO_x catalysts. (B) FTIR spectra of $Mn_6Ce_{0.3}In_{0.7}O_x$ and Mn_6CeO_x catalysts treated in simulated flue gas at 150 °C for 60 min. Reaction conditions: 500 ppm NH_3, 500 ppm NO, 5 vol % O_2, 5 vol % H_2O, 100 ppm SO_2, and balance N_2 (GHSV = 120,000 h^{-1}).

Other metal oxides have been added to further improve their low-temperature activity and stability. Because of its excellent redox performance, cerium was used as an enhancer to dope the original catalyst to improve the catalyst activity.[12] Li et al. prepared Mn−CeO_x nanospheres using the geothermal approach with excellent denitrification performance but only at low space velocity.[13] Andreoli et al. prepared a MnO_x-CeO_x catalyst through the amino acetic acid method.[14] Although it has an excellent conversion rate at 150−280 °C, its selectivity is poor. Although cerium has improved the sulfur resistance of the MnO_x catalyst, it still needs to be further improved.[15−17] Decolatti et al. synthesized In-NH_4-zeolites and found that indium species could promote the oxidation of NO to NO_2. The higher the indium content meant the better the denitrification effect.[18] Pan et al. found that surface indium species can react with SO_2 and H_2O to produce $In_2(SO_4)_3$.[19] It was found that the low-temperature denitrification performance could be significantly improved by H_2 treatment at 400 °C for 60 min, although the sulfate radical could not be completely removed.

In this work, the denitrification performance of $MnCeO_x$ and $MnCeInO_x$ catalysts with different ratios of In and the stability in the presence of water vapor and SO_2 have been tested using an NH_3-SCR denitrification device at 100−275 °C. The gas hourly space velocity (GHSV) was 120,000 h^{-1}. The catalysts were characterized by FTIR, SEM, XRD, BET, XPS, H_2-TPR, and NH_3-TPD. The possible reaction pathways were studied.

2. RESULTS AND DISCUSSION

2.1. Catalyst Performance Analysis. Figure 1 shows the NO_x conversion efficiency of $MnCeO_x$ and a series of $MnCeInO_x$ with different proportions. The T80 (NO_x conversion efficiency of >80%) of Mn_6CeO_x is at 125−200

https://doi.org/10.1021/acsomega.1c07000
ACS Omega 2022, 7, 6381−6392

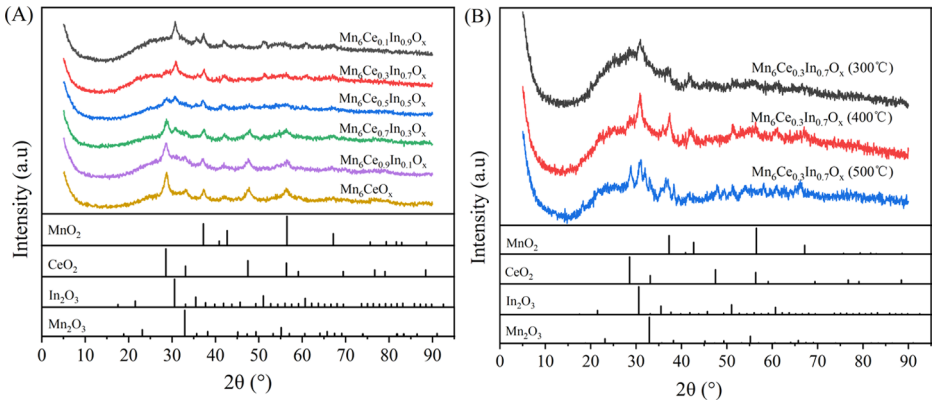

Figure 3. (A) XRD results of $MnCeO_x$ and $MnCeInO_x$ series. (B) XRD results of the $Mn_6Ce_{0.3}In_{0.7}O_x$ catalyst at different calcination temperatures.

°C, and the highest conversion rate is 91.2%. When Ce:In = 3:7, the catalyst shows the best conversion efficiency of T90 in the range of 125−225 °C and the best conversion rate is 94.5%. This not only enlarges the Mn_6CeO_x temperature operating window but also improves the conversion efficiency. It can also be seen from Figure 1B that compared with the Mn_6CeO_x catalyst, doping of indium also improves the selectivity of N_2. Figure 1C shows the effect of different calcination temperatures and different space velocities for the NO_x conversion efficiency with the $Mn_6Ce_{0.3}In_{0.7}O_x$ catalyst. As shown by the figure, when the space velocity is too high, the conversion efficiency of the catalyst decreases significantly. When the space velocity decreases, the catalyst conversion rate increases further in the range of 100−175 °C, indicating that increasing the volume of the catalysts could increase the number of active sites and facilitate the processing of more feed gas. The calcination temperature has a great influence on the conversion efficiency of the catalyst. At 300 °C, the catalyst showed poor catalytic activity, the best conversion rate was only 90.8%, and T80 had a temperature operating window of 125−250 °C. When the calcination temperature is 500 °C, the conversion efficiency of the catalyst is slightly lower than the calcination temperature of 400 °C but its T90 still has a wide temperature operating window of 125−225 °C. It can be seen from the XRD diagram that the crystallization of the catalyst after calcination at 500 °C is higher than the other two calcination temperatures, which leads to the agglomeration of CeO_2 at the catalyst surface and the generation of more Mn_2O_3, affecting the catalytic efficiency. XRD patterns at a calcination temperature of 300 °C showed wide and mixed peaks, indicating that the catalyst was poorly formed and not fully calcined.

Figure 2A shows the water and sulfur resistance test results of $Mn_6Ce_{0.3}In_{0.7}O_x$ and Mn_6CeO_x catalysts at 150 °C. First of all, the catalyst was stably exposed to raw gas at 150 °C for 1 h, 5% H_2O was passed through the catalyst for continuous testing for 5 h, and then, the water vapor was closed. Then, 100 ppm SO_2 was passed one hour after catalyst recovery, SO_2 was closed after the continuous test for 5 h, and then, we waited for recovery for another hour. On this basis, 5% H_2O and 100 ppm SO_2 were added simultaneously, water vapor and SO_2 were closed after 5 h of monitoring, and the recovery of the catalytic efficiency was detected for 1 h.

In practical engineering applications, H_2O and SO_2 are the influencing factors that cannot be ignored. The sulfurization of catalysts and the formation of NH_4HSO_4 are the key reasons leading to the reduction of catalytic efficiency of catalysts.[22] In Figure 2A, the water resistance of the two catalysts is similar, and the conversion rate decreases by 8%. After H_2O is closed, $Mn_6Ce_{0.3}In_{0.7}O_x$ shows a stronger recovery ability than the Mn_6CeO_x catalyst, and the conversion efficiency of $Mn_6Ce_{0.3}In_{0.7}O_x$ returns to the state before water is added. The Mn_6CeO_x catalyst recovered 5%. When 100 ppm SO_2 was introduced, the catalytic efficiency of $Mn_6Ce_{0.3}In_{0.7}O_x$ suddenly dropped, which may be due to part of the active sites on the catalyst surface being covered by sulfide or ammonium sulfate when SO_2 was passed through the catalyst in the early stage. After 1 h of SO_2 induction, the catalytic efficiency recovered 91.6%, which was related to the decomposition of ammonium sulfate on the catalyst surface, releasing part of the active sites and causing the efficiency of the catalyst to rebound. Then, the conversion rate gradually decreased to 89.4% with the increase in time and recovered 93% after the closure of SO_2. The catalytic efficiency of Mn_6CeO_x decreased gradually with the increase in time, decreased to 76% after 5 h, and recovered 81.5% after closing SO_2. When the water and sulfur resistance of the two catalysts was tested, $Mn_6Ce_{0.3}In_{0.7}O_x$ showed a better effect than Mn_6CeO_x. The conversion efficiency of $Mn_6Ce_{0.3}In_{0.7}O_x$ and Mn_6CeO_x decreased to 82.4 and 67% after the 5 h test, respectively. The conversion efficiency of $Mn_6Ce_{0.3}In_{0.7}O_x$ and Mn_6CeO_x recovered 87.2 and 70.7% after water vapor and SO_2 were closed, respectively. The addition of indium significantly improved the resistance ability of the Mn_6CeO_x catalyst to H_2O and SO_2. According to the recovery ability of the $Mn_6Ce_{0.3}In_{0.7}O_x$ catalyst after the test of sulfur resistance, SO_2 had little effect on it, and the main effect was from water vapor. The influence on the recovery ability of the two catalysts through the H_2O and SO_2 resistance tests revealed that a part of the active site of the catalyst may be covered by $(NH_4)_2SO_4$.

To obtain the difference of the surface structure of the catalysts after the water and sulfur resistance test, the catalysts were characterized by Fourier transform infrared spectroscopy (FTIR). Figure 2B shows the FTIR spectra of $Mn_6Ce_{0.3}In_{0.7}O_x$ and Mn_6CeO_x catalysts after H_2O and SO_2 resistance tests. In FTIR tests of the Mn_6CeO_x catalyst, 3414 cm^{-1} was attributed to the vibration of the O−H bond of H_2O.[23,24] In the FTIR test of the $Mn_6Ce_{0.3}In_{0.7}O_x$ catalyst, 3390 cm^{-1} was attributed to the N−H tensile vibration mode of NH_3.[24,25] According to literature reports, 3200 cm^{-1} was attributed to the formation with other forms of NH_3 and NH_4^+.[24] The 1631−1627 cm^{-1} peak belongs to adsorbed NO_2.[26] The 1450−1443 cm^{-1} peak belongs to NH_4^+ formed by adsorption at the Brønsted acidic sites.[27,28] The 1400−1383 cm^{-1} peak was attributed to

https://doi.org/10.1021/acsomega.1c07000
ACS Omega 2022, 7, 6381−6392

ammonium sulfate[29] and 1114−1070 cm^{-1} to sulfate.[30] The 1265 cm^{-1} peak was attributed to monotonic nitrite.[31] The 863−862 cm^{-1} peak belongs to physical adsorption or weak phase adsorption of NH_3. In the wavelength range of less than 800 cm^{-1}, it belongs to the vibration between metal and oxygen atoms, and 558−569 cm^{-1} was related to the vibration of the Mn−O bond.[32] By comparing the results of the two catalysts, the two catalysts both contain single-toothed nitrate, adsorbed NO_2, adsorbed NH_3, and NH_4^+ but do not contain double-toothed nitrate. In addition, they all contain ammonium sulfate and sulfate. The results showed that SO_2 inhibited the formation of nitrates on the Mn_6CeO_x catalyst and had little effect on the adsorption of nitrates and ammonia on the monotone. It is not difficult to see that the peak intensity of ammonium sulfate and sulfate on the $Mn_6Ce_{0.3}In_{0.7}O_x$ catalyst decreases obviously in the FTIR diagram, and the peak intensity increases in the range of 3000−3750 cm^{-1}, which indicates that indium doping could effectively reduce the formation of ammonium sulfate and sulfate at the catalyst. Moreover, it can improve the chemisorption of NH_3 and the formation of NH_4^+.

2.2. XRD Analysis. Figure 3A presents the XRD results for the $MnCeO_x$ and $MnCeInO_x$ series. According to JADE 6 software, the Mn_6CeO_x sample contains sharp XRD peaks of the MnO_2 phase (PDF no. 89-5171) and the CeO_2 phase (PDF no. 34-0394). The presence of MnO_2, CeO_2, In_2O_3, and Mn_2O_3 (PDF no. 24-0508) phases can be observed in the $MnCeInO_x$ series. With the decrease in the cerium content and the increase in the indium content, the XRD peak of the CeO_2 phase becomes weaker, and the peak strength of 37.2° of the (100) crystal of MnO_2 gets stronger. With the increase in the indium content, the (102) plane diffraction peak at 56.47° of MnO_2 decreases gradually, indicating that MnO_x exists as an amorphous component.[33] The results indicated that indium was doped to inhibit the crystallization of CeO_2 and promote the growth of the MnO_2(100) crystal. At the same time, the In_2O_3 phase (PDF no. 22-0336) gradually appeared, indicating that the In_2O_3 structure formed on the surface of $MnCeO_x$.

In Figure 3B, the calcination temperatures of $Mn_6Ce_{0.3}In_{0.7}O_x$ catalysts were compared. The catalysts calcined at 300 °C have obvious diffraction peaks between 30 and 45° but no diffraction peaks in other ranges. It indicates that the catalyst is not fully formed. The catalyst calcined at 500 °C has an obvious diffraction peak of CeO_2 at 2θ = 28°, which indicates that the dispersed cerium can be condensed by calcination at high temperatures. At 2θ = 33°, the Mn_2O_3 crystal peak is formed, indicating that more Mn_2O_3 is produced on the surface of the catalyst by calcination at high temperatures. The agglomeration of CeO_2 and more Mn^{3+} negatively affects the performance of the catalyst. Combined with the denitration test results, studies showed that the catalyst calcined at 300 °C had the worst NO_x conversion, the efficiency was slightly better at 500 °C, and the efficiency was the best at 400 °C. In summary, the preparation temperature of calcination at 400 °C is the best preparation temperature for the catalyst.

2.3. SEM Result Analysis. Figure 4 shows the SEM morphology of (a−c) $Mn_6Ce_{0.3}In_{0.7}O_x$ and (d−f) Mn_6CeO_x catalysts. The comparison of Figure 4a and Figure 4d shows that the Mn_6CeO_x catalyst with more cerium content has many CeO_2 flakes dispersed around spherical MnO_x. $Mn_6Ce_{0.3}In_{0.7}O_x$ is spherical in various sizes and contains a small amount of CeO_2 flakes. According to the comparison of

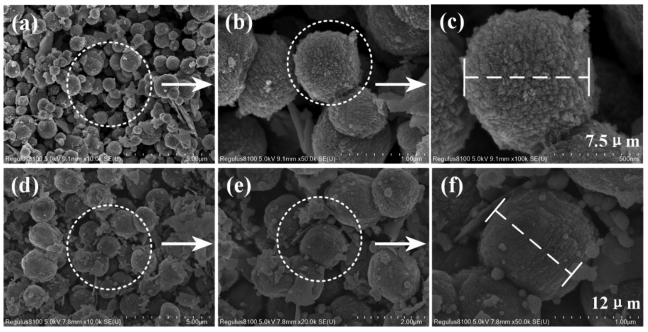

Figure 4. SEM morphology of (a−c) $Mn_6Ce_{0.3}In_{0.7}O_x$ and (d−f) Mn_6CeO_x catalysts.

Figure 4c and Figure 4f, the particle diameter of the $Mn_6Ce_{0.3}In_{0.7}O_x$ catalyst is 7.5 μm, and the surface of the $Mn_6Ce_{0.3}In_{0.7}O_x$ catalyst is uneven and covered like microvilli. The particle diameter of the Mn_6CeO_x catalyst is 12 μm, and the surface appears smooth and flat. The addition of indium changed the appearance and size of the Mn_6CeO_x catalyst, which increased the specific surface area of the $Mn_6Ce_{0.3}In_{0.7}O_x$ catalyst.

2.4. Variation of the Specific Surface Area and the Pore Structure. Importantly, a larger specific surface area can provide more catalytic active sites and reaction paths for SCR catalytic reactions. The SEM results indicated that the morphology of the two catalysts also changed, so the difference between them was quantitatively studied by the N_2 adsorption/desorption isothermal curve and pore size distribution. Figure 5 presents the nitrogen adsorption/

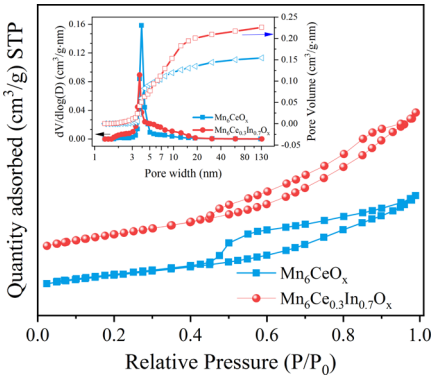

Figure 5. N_2 physisorption isotherms and pore size distribution of $Mn_6Ce_{0.3}In_{0.7}O_x$ and Mn_6CeO_x catalysts.

desorption isotherm and pore size distribution of $Mn_6Ce_{0.3}In_{0.7}O_x$ and Mn_6CeO_x catalysts. Both catalysts exhibit a typical type IV isotherm, indicating that both materials are mesoporous. By comparing the hysteresis loop, the two catalysts showed obvious differences. The Mn_6CeO_x catalyst exhibits a typical H4-type hysteresis loop and has significant adsorption capacity at the low end of P/P_0, indicating that its pore structure is narrow and fractured.[34] The $Mn_6Ce_{0.3}In_{0.7}O_x$ catalyst exhibits an isotherm type of the H3 hysteresis loop at a high relative pressure between 0.8 and 0.99, indicating that the surface of the catalyst has a mesoporous structure with flat slit channels. The difference can also be seen by considering the pore size distribution in Figure 6. The pore size distribution of the $Mn_6Ce_{0.3}In_{0.7}O_x$ catalyst is between 2 and 20 nm, and the pore volume distribution is between 0 and 0.23 $cm^3/g{\cdot}nm$. The

https://doi.org/10.1021/acsomega.1c07000
ACS Omega 2022, 7, 6381−6392

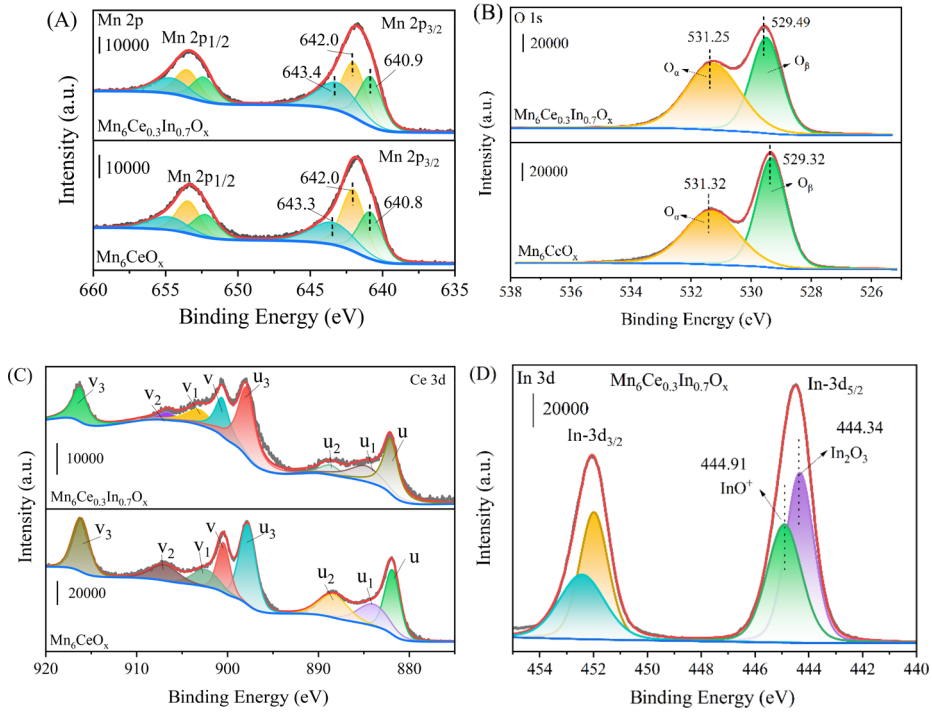

Figure 6. XPS Mn 2p (A), O 1s (B), Ce 3d (C), and In 3d (D) spectra of Mn_6CeO_x and $Mn_6Ce_{0.3}In_{0.7}O_x$ catalysts.

pore size and volume distributions of the Mn_6CeO_x catalyst are 3−18 nm and 0−0.15 $cm^3/g{\cdot}nm$, respectively. Table 1 lists the

Table 1. BET Specific Surface Area and Pore Characterization of the Samples

samples	BET surface area (m^2/g)	pore volume (cm^3/g)	pore diameter (nm)
Mn_6CeO_x	113.7	0.15	3.9
$Mn_6Ce_{0.3}In_{0.7}O_x$	140.7	0.23	3.7

specific surface area, pore volume, and pore size of $Mn_6Ce_{0.3}In_{0.7}O_x$ and Mn_6CeO_x catalysts. Although the pore size of the catalyst decreases with indium doping, the specific surface area increases by 23.7%. The results are consistent with those of the hysteresis loop and SEM. Therefore, the doping of indium increases the pore volume of the catalyst, increases the surface area of the catalyst, and provides more catalytic active sites.

2.5. Analysis of Surface Element Valence States. In order to understand the properties of elements on the catalyst surface, XPS tests were carried out on $Mn_6Ce_{0.3}In_{0.7}O_x$ and Mn_6CeO_x catalysts, as shown in Figure 6. The Mn 2p, O 1s, Ce 3d, and In 3d spectra of the catalyst were fitted by XPSPEAK4.1. Figure 6A shows the deconvoluted peaks of Mn 2p for catalysts $Mn_6Ce_{0.3}In_{0.7}O_x$ and Mn_6CeO_x. The XPS spectra of the Mn 2p region showed a pair of peaks for all the samples, which were attributed to Mn $2p_{3/2}$ and Mn $2p_{1/2}$, respectively. Three peaks of Mn $2p_{3/2}$ of the two catalysts can be observed (Figure 6A): Mn^{2+} (640.9−640.8 eV), Mn^{3+} (642.0 eV), and Mn^{4+} (643.4−643.3 eV).[34−36] Mn ions in $Mn_6Ce_{0.3}In_{0.7}O_x$ have a variety of valence states, which makes it easy to form a redox pair of $Mn^{n+}/Mn^{(n+1)+}$, causing a good NH_3-SCR activity. The relative proportion of Mn^{4+} in the indium-doped $Mn_6Ce_{0.3}In_{0.7}O_x$ catalyst increased compared to Mn_6CeO_x (Table 2). Corresponding to the XRD results, the increase in the high valence state of Mn enhances the oxidation capacity of the $Mn_6Ce_{0.3}In_{0.7}O_x$ catalyst, thus improving the SCR performance.

Figure 6B shows the deconvoluted XPS spectra of O 1s in Mn_6CeO_x and $Mn_6Ce_{0.3}In_{0.7}O_x$ catalysts. The peak at 529.49 eV corresponds to the lattice oxygen O^{2-} (O_β). The peaks at 530.5−531.3 eV correspond to surface oxygen (O_α), such as groups belonging to defective oxides and hydroxyl oxygen (e.g., O_2^{2-} or O^-).[37−39] Since O_α is more reactive and migrates more easily than O_β, it could contribute to the oxidation of NO to NO_2 in the SCR reaction, allowing the catalyst to exhibit a better performance in the oxidation reaction.[40−42] The calculated O_α ratio of the $Mn_6Ce_{0.3}In_{0.7}O_x$ catalyst is shown in Table 2. The surface oxygen O_α content of the $Mn_6Ce_{0.3}In_{0.7}O_x$ catalyst (54.71%) is higher than that of Mn_6CeO_x (47.17%), indicating that the $Mn_6Ce_{0.3}In_{0.7}O_x$ catalyst has more surface oxygen O_α than the Mn_6CeO_x catalyst, which is beneficial for fast SCR reactions ($4NH_3 + 2NO + 2NO_2 \rightarrow 4\ N_2 + 6H_2O$) at low temperatures.

Figure 6C shows the fitting spectrum of Ce 3d. The XPS spectra of the Ce 3d region showed a pair of peaks for all the samples, which were attributed to Ce $3d_{5/2}$ and Ce $3d_{3/2}$, denoted by "u" and "v" corresponding to the spin−orbit

Table 2. Surface Element Valence States and Relative Contents of Mn, O, and Ce

samples	Mn^{2+}/Mn	Mn^{3+}/Mn	Mn^{4+}/Mn	O_α/O	O_β/O	Ce^{3+}/Ce	Ce^{4+}/Ce
Mn_6CeO_x	31.5%	41.1%	27.4%	47.2%	52.8%	18.3%	81.7%
$Mn_6Ce_{0.3}In_{0.7}O_x$	32.3%	36.4%	31.3%	54.7%	45.3%	21.1%	78.9%

https://doi.org/10.1021/acsomega.1c07000
ACS Omega 2022, 7, 6381−6392

component of Ce $3d_{5/2}$ and Ce $3d_{3/2}$, respectively. It can be observed that there are 8 peaks of u, u_1, u_2, u_3, v, v_1, v_2, and v_3 for Ce 3d where v_1 and u_1 are Ce^{3+} and the other peaks are Ce^{4+}.[29,43,44] On the whole, the cerium element in the two catalysts mainly exists in the form of Ce^{4+} ions, and only a small amount of Ce^{3+} exists. In Table 2, the Ce^{3+}/Ce ratios of $Mn_6Ce_{0.3}In_{0.7}O_x$ and Mn_6CeO_x catalysts are 21.1 and 18.3%, respectively. It indicates that the doping of indium leads to the decrease in the relative content of Ce^{4+}, which is because the In^{3+} ions inserted into the catalyst replace the position of Ce^{4+}, thus changing the oxygen content in the sintering process of the catalyst, transforming Ce^{4+} into Ce^{3+}.[45] Increasing the concentration of Ce^{3+} at the catalyst surface can promote the formation of charge imbalance, unsaturated bonds, and vacancies.[33,46] Therefore, the following processes may occur between Ce^{4+} and Ce^{3+} on the catalyst surface in the SCR reaction: (1) $2CeO_2 \rightarrow Ce_2O_3 + O^*$ and (2) $Ce_2O_3 + 1/2O_2 \rightarrow 2CeO_2$.[29,47] In this process, the oxygen in the flue gas is adsorbed and dissociated on the catalyst surface through the oxygen vacancy to produce oxygen with high fluidity and promote the oxidation of NO to NO_2.

Figure 6D shows the deconvolution of the In $3d_{5/2}$ signal, and two peaks can be obtained, namely, a binding energy of 444.34 eV(structure related to In_2O_3 species) and a binding energy of 444.91 eV (structure similar to InO^+ species).[48,49] Surface $(InO)^+$ is considered to be the active site in the SCR reaction. The active site can bind to gaseous NH_3 to form adsorbed ammonia and then dissociate NH_3 to form $-NH_2$ and $[In(OH)_x]^{n+}$,[50] and the formation of these groups contributes to the fast SCR reaction.

2.6. Redox Property. The redox capacity of the catalyst was characterized by H_2 temperature-programmed reduction (H_2-TPR). It is shown in Figure 7. After the split peak, it was

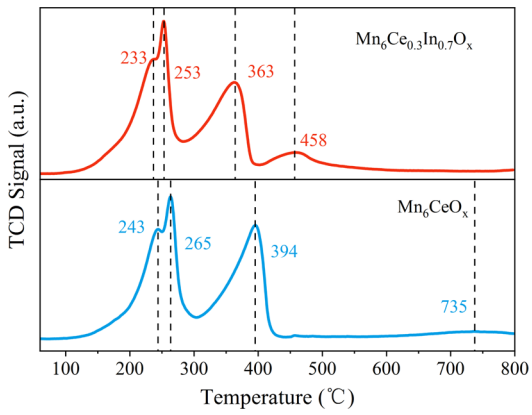

Figure 7. H_2-TPR profiles of catalysts.

observed that there are four reduction peaks for Mn_6CeO_x and $Mn_6Ce_{0.3}In_{0.7}O_x$ catalysts. By comparing the H_2 reduction curves of the two catalysts, the peaks of Mn_6CeO_x in the range of 100−300 °C can be divided into three peaks centered at 243, 265, and 394 °C. These three reduction peaks correspond to the reduction of MnO_2 to nonstoichiometric dispersed MnO_x ($1.5 < x < 2$). At this point, the exposed high flow of oxygen on the catalyst surface was removed. MnO_x is then reduced to Mn_2O_3, at which time part of the lattice oxygen on the catalyst surface decreases. Finally, Mn_2O_3 is reduced to Mn_3O_4 and further to MnO.[51−53] Chen et al.[54] reported that the surface Ce^{4+} to Ce^{3+} reduction process also occurred at 394 °C. A very low and flat peak was observed at the center of 735 °C. According to the literature, the peak in the range of temperature more than 700 °C corresponds to the reduction of the surface and bulk of cerium oxide.[55]

Compared with the Mn_6CeO_x catalyst, the $Mn_6Ce_{0.3}In_{0.7}O_x$ catalyst exhibited a similar reduction peak in the temperature range of less than 400 °C. However, the peak values of these reduction peaks all shifted to the direction of low temperatures. The results indicate that the surface of the Mn_6CeO_x catalyst doped with indium is more prone to electron transfer, indicating that the catalyst has a lower SCR activity temperature, thus improving the catalytic performance. Peaks greater than 700 °C were not observed, possibly due to a decrease in the cerium content. There was no reduction peak, or the reduction peak moved to a higher-temperature region, which to some extent reduced the oxidation of cerium in the catalyst, inhibited the formation of nitrous oxide, and reduced the nonselective catalytic oxidation of NH_3. This may be one of the reasons for increased N_2 selectivity. It can be seen that a new reduction peak is added at 458 °C, which is considered to be the indium phase prone to surface reduction, such as $(InO)^+$ and In_xO_y,[19,56] as shown in the following formula:

$$In_xO_y + xH_2 + xH^+M^- \rightarrow xIn^+M + yH_2O \quad (6)$$

$$(InO)^+ + H_2 \rightarrow In^+ + H_2O \quad (7)$$

After indium doping, indium enters into the lattice of MnO_2, and the interaction between the components of the catalyst promotes the reduction of manganite and indium ions, improving the catalytic performance of the SCR catalyst. The reported H_2 unit consumption of the catalyst Mn_6CeO_x (7.41 $\mu mol \cdot g^{-1}$) was less than that of $Mn_6Ce_{0.3}In_{0.7}O_x$ (8.62 $\mu mol \cdot g^{-1}$). The results showed that the reduction peak positions of the two catalysts were not significantly different, but the reduction peaks shifted to low temperatures, indicating that indium doping improved the reduction properties of the Mn−Ce oxides to some extent, which was beneficial to the denitrification performance of the catalyst.

2.7. Acidity of the Catalysts. The acidity of Mn_6CeO_x and $Mn_6Ce_{0.3}In_{0.7}O_x$ catalysts was studied by NH_3-TPD experiments, as shown in Figure 8. The amount and intensity of acid sites at the catalyst surface and the activation of NH_3 at the catalyst surface were measured by the NH_3-TPD technique. In the temperature range of 50−800 °C, Origin 2021 software Gaussian fitting was used to obtain six analytical

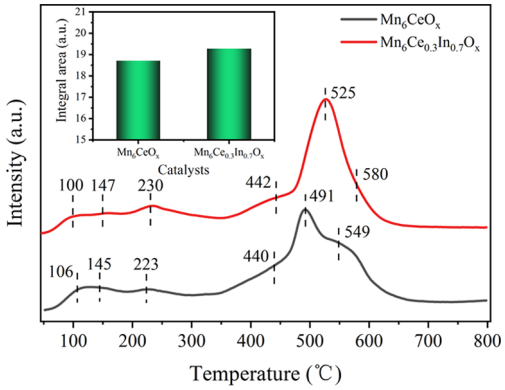

Figure 8. NH_3-TPD profiles of Mn_6CeO_x and $Mn_6Ce_{0.3}In_{0.7}O_x$ catalysts.

https://doi.org/10.1021/acsomega.1c07000
ACS Omega 2022, 7, 6381−6392

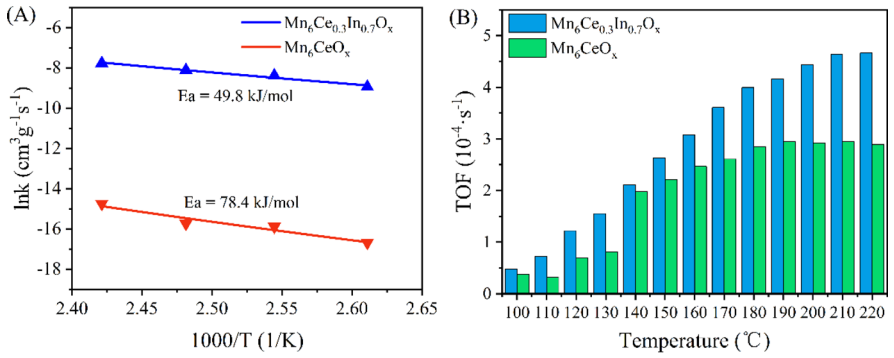

Figure 9. (A) Arrhenius plots of $Mn_6Ce_{0.3}In_{0.7}O_x$ and Mn_6CeO_x catalysts. (B) TOF over $Mn_6Ce_{0.3}In_{0.7}O_x$ and Mn_6CeO_x catalysts at different temperatures.

peaks for catalysts Mn_6CeO_x and $Mn_6Ce_{0.3}In_{0.7}O_x$. These peaks consisted of peak 1 (100 and 106 °C), peak 2 (147 and 145 °C), peak 3 (230 and 223 °C), peak 4 (442 and 458 °C), peak 5 (525 and 492 °C), and peak 6 (580 and 548 °C). According to literature reports, below 350 °C is a weak acid site, and above 350 °C is a medium-strong acid site.[57,58] Peaks 1, 2, and 3 belong to weak acid sites, which are composed of physical or weak chemical adsorption of NH_3 and NH_4^+ produced by the combination of NH_3 and surface hydroxyl groups. Peaks 4, 5, and 6 belong to medium-strong acid sites and are caused by the adsorption of NH_3 at the Brønsted or Lewis acid sites. It is well-known that the desorption peak position and the desorption peak area of a catalyst correspond to the strength and quantity of the acid, respectively.[59] The amount of surface acid sites of Mn_6CeO_x and $Mn_6Ce_{0.3}In_{0.7}O_x$ catalysts can be estimated after integrating the NH_3-TPD curves. The integral area shown in Figure 8 indicated that the acid content of the Mn_6CeO_x catalyst was 18.7 μmol·g^{-1}, which was less than that of the $Mn_6Ce_{0.3}In_{0.7}O_x$ catalyst (19.3 μmol·g^{-1}). The results showed that the doping of indium in Mn_6CeO_x catalysts could improve the number of surface acid sites and enhance the adsorption of NH_3 on the catalysts to a certain extent.

2.8. Kinetic Study. Arrhenius plots of $Mn_6Ce_{0.3}In_{0.7}O_x$ and Mn_6CeO_x catalysts in the range of 110−140 °C are shown in Figure 9A. The turnover frequency (TOF) of $Mn_6Ce_{0.3}In_{0.7}O_x$ and Mn_6CeO_x catalysts in the range of 100−220 °C is shown in Figure 9B. The test method was to fully mix 0.01 g of the catalyst and 0.09 g of SiO_2 for testing in an NH_3-SCR evaluation device to ensure that the reactivity was not affected by diffusion.[21,60] It can be seen from Figure 9A that the apparent activation energy (E_a) of the $Mn_6Ce_{0.3}In_{0.7}O_x$ catalyst (49.8 kJ /mol) is less than that of Mn_6CeO_x (78.4 kJ /mol), indicating that it is easier for the $Mn_6Ce_{0.3}In_{0.7}O_x$ catalyst to promote the reaction than Mn_6CeO_x. In Figure 9B, the TOF value of the $Mn_6Ce_{0.3}In_{0.7}O_x$ catalyst increased as the temperature increased. The higher the temperature value, the higher the TOF value and the better the SCR activity, which finally tended to balance after 200 °C. The TOF value of the Mn_6CeO_x catalyst also increased with the increase in temperature and reached the maximum value at 190 °C and then gradually decreased. This is the same as its SCR activity.

2.9. Discussion. The results show that the $MnCeO_x$ catalyst has a temperature operating window of T80 of 125−200 °C at GHSV = 120,000 h^{-1} and shows good activity but poor activity in other temperature test sections. The activation of the $MnCeO_x$ catalyst was promoted by adding indium. For example, the temperature window of the catalyst T90 increases from 150−175 to 125−225 °C. The activation energy of the $Mn_6Ce_{0.3}In_{0.7}O_x$ catalyst is lower than that of the Mn_6CeO_x catalyst obtained from the Arrhenius plot (Figure 10A) results.

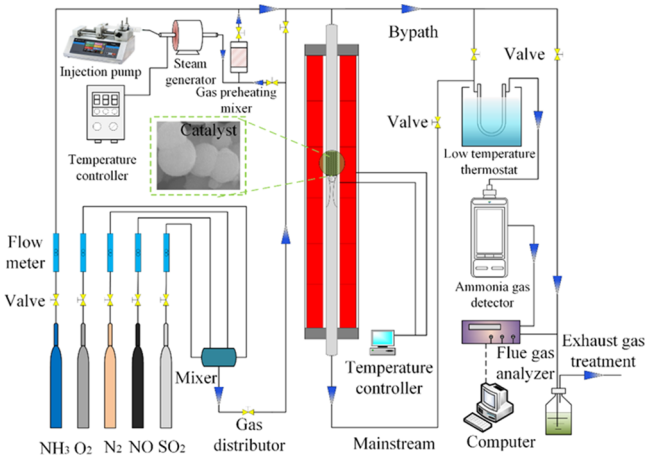

Figure 10. Schematic flowchart of the catalytic activity in the evaluation device.

In the range of 100−220 °C, the TOF value calculated based on NH_3-TPD data (Figure 10B) is larger for the $Mn_6Ce_{0.3}In_{0.7}O_x$ catalyst. The results showed that the doping of indium could effectively improve the synergistic interaction between active sites, increase the TOF value of the Mn_6CeO_x catalyst, and improve the catalytic performance of the catalyst. $Mn_6Ce_{0.3}In_{0.7}O_x$ and Mn_6CeO_x catalysts have been compared in water and sulfur resistance tests (Figure 2A). It can be found that both catalysts show a good recovery ability in water resistance tests. In addition, $Mn_6Ce_{0.3}In_{0.7}O_x$ showed a better sulfur resistance than $Mn_6Ce_{0.3}In_{0.7}O_x$, and neither of the two catalysts returned to the state before adding SO_2. The $Mn_6Ce_{0.3}In_{0.7}O_x$ catalyst has more obvious advantages when both H_2O and SO_2 are present and has a small reduction in catalytic efficiency and good stability. According to the FTIR results of the tested catalyst (Figure 2B), $Mn_6Ce_{0.3}In_{0.7}O_x$ showed a better water and sulfur resistance because indium distributed on the catalyst surface reduced the content of sulfate on the surface and protected the acidic site of MnCe. XRD test results (Figure 3) showed that indium doping inhibited the crystallization of CeO_2 and promoted the growth of the MnO_2(100) crystal plane. The results showed that amorphous CeO_2 and more MnO_2(100) crystal surfaces were

https://doi.org/10.1021/acsomega.1c07000
ACS Omega 2022, 7, 6381−6392

helpful to improve the activity of the catalyst. In the XRD results of different calcination temperatures, it can be found that the crystallization of the catalyst calcined at 300 °C was bad. The crystallization of the 400 °C calcined catalyst was excessive. The results showed that the crystallinity of the catalyst had a significant effect on the catalytic activity. It can be seen from the SEM images and specific surface area and pore size test results that the doping of indium changes the morphology and size of catalyst particles, increases the specific surface area and pore capacity of the catalyst, and thus provides more surface acid sites. XPS characterization was conducted to understand the surface element valence, surface oxygen state, acidity, and reducibility of the catalyst and then speculate the catalytic process of the catalytic reaction. The XPS test results show that the $Mn_6Ce_{0.3}In_{0.7}O_x$ catalyst has a higher proportion of Mn^{4+} and surface oxygen (O_α) than the Mn_6CeO_x catalyst, which improves the catalytic oxide behavior and improves the SCR performance. In the $Mn_6Ce_{0.3}In_{0.7}O_x$ catalyst, the In^{3+} ions replace the position of Ce^{4+}, resulting in the relative increase in the Ce^{3+} content and surface oxygen defects.[45] This oxygen vacancy can make the oxygen in the flue gas adsorbed and dissociated over the catalyst surface to produce oxygen with high flow and promote the oxidation of NO to NO_2. In the reduction test, the reduction peak temperature of the $Mn_6Ce_{0.3}In_{0.7}O_x$ catalyst was reduced, indicating that the SCR activity temperature of the $Mn_6Ce_{0.3}In_{0.7}O_x$ catalyst was reduced, which is consistent with the calculation of the apparent activation energy. At around 700 °C, the hydrogen reduction curve of the $Mn_6Ce_{0.3}In_{0.7}O_x$ catalyst did not show the reduction peak of cerium, indicating that the oxidation of the catalyst was reduced to some extent and the N_2O production was inhibited. In the test of surface acidity, the $Mn_6Ce_{0.3}In_{0.7}O_x$ catalyst showed enhanced surface acid site intensity and increased adsorption capacity for NH_3, indicating that more NH_3 was activated or decomposed on its surface and participated in the SCR denitrification reaction. In summary, the doping of the indium element increases the proportion of active centers due to the increase in the specific surface area of the catalyst. In addition, indium improves the intensity and the number of acidic sites to some extent and enhances the synergistic effect between multivalent cationic active centers in the SCR reaction, thus improving the catalytic efficiency.

According to the existing reports,[27,61−63] the current mainstream view is that the low-temperature NH_3-SCR reaction on the surface of a manganese-based catalyst follows the reaction process dominated by the Eley−Rideal (E−R) mechanism and supplemented by the Langmuir−Hinshelwood (L−H) mechanism. Therefore, the reaction process on the surface of the $Mn_6Ce_{0.3}In_{0.7}O_x$ catalyst was inferred according to XPS elemental valence analysis. It can be expressed as follows: NH_3 is adsorbed forming Lewis acid sites to adsorb ammonia. NH_3 is further dissociated to NH_4^+ and adsorbed NH_2 on the surface of the catalyst forming Brønsted acid sites and reacts with gaseous NO or NO_2 to generate the intermediate products NH_2NO, NH_4NO_2, and NH_4NO_3. On the other hand, oxygen was activated combined with NO or NO_2 in the raw gas at the oxygen defect at the catalyst surface and then reacted with adsorbed NH_4^+ at Brønsted acid sites to produce intermediate products NH_4NO_2 and NH_4NO_3. NH_2NO and NH_4NO_2 were further decomposed into nitrogen and water due to instability, and NH_4NO_3 will further combine with NO to generate NH_4NO_2 and NO_2 at low temperatures. As the temperature increases, NH_4NO_3 will decompose into H_2O and harmful gas N_2O. The possible reaction process on the surface of the $Mn_6Ce_{0.3}In_{0.7}O_x$ catalyst is given by the following:

$$InO + NH_3(g) \rightarrow InOH + NH_2(ad) \quad (8)$$

$$InOH + NH_3(g) \rightarrow In - O - NH_4(ad) \quad (9)$$

$$MnO_x + O_2(g) \rightarrow MnO_x + 2O(ad)(1.5 < x < 2) \quad (10)$$

$$CeO_x + O_2(g) \rightarrow CeO_x + 2O(ad)(1.5 < x < 2) \quad (11)$$

$$2NO(g) + O_2(g) \rightarrow 2NO_2(g) \quad (12)$$

$$NO(g) + O(ad) \rightarrow NO_2(ad) \quad (13)$$

$$NO_2(g) + O(ad) \rightarrow NO_3(ad) \quad (14)$$

$$NH_2(ad) + NO(g) \rightarrow NH_2NO(ad) \rightarrow N_2(g) + H_2O(g) \quad (15)$$

$$NH_4(ad) + NO_2(ad) \rightarrow NH_4NO_2(ad) \quad (16)$$

$$NH_4(ad) + NO_2(g) \rightarrow NH_4NO_2(ad) \quad (17)$$

$$NH_2(ad) + NO_2(g) \rightarrow NH_2NO_2(ad) \rightarrow N_2O(g) + H_2O(g) \quad (18)$$

$$NH_4(ad) + NO_3(ad) + NO(g) \rightarrow NH_4NO_2(ad) + NO_2(g) \quad (19)$$

$$NH_4(ad) + NO_3(ad) \rightarrow NH_4NO_3(ad) \quad (20)$$

$$NH_4NO_2(ad) \rightarrow N_2(g) + 2H_2O(g) \quad (21)$$

$$NH_4NO_3(ad) \rightarrow N_2O(g) + 2H_2O(g) \quad (22)$$

$$2InOH + O(ad) \rightarrow InO + H_2O(g) \quad (23)$$

3. CONCLUSIONS

$MnCeInO_x$ catalysts were prepared for NH_3-SCR by a coprecipitation method. The test results showed that $Mn_6Ce_{0.3}In_{0.7}O_x$ exhibited the best catalytic activity at low temperatures, and its optimal preparation temperature was 400 °C. The temperature window for denitrification efficiency greater than 90% (T90) was extended from 150−175 to 125−225 °C. The $Mn_6Ce_{0.3}In_{0.7}O_x$ catalyst had a low apparent activation energy (E_a) and a high turnover frequency (TOF) compared to the undoped catalyst without indium, indicating that the doping of indium improved the synergistic effect of the catalyst active sites. In addition, indium doping reduced the formation of sulfate on the catalyst and enhanced the water and sulfur resistance of the Mn_6CeO_x catalyst. The denitrification efficiency of the $Mn_6Ce_{0.3}In_{0.7}O_x$ catalyst was higher than that of Mn_6CeO_x by 15.4% after a 5 h test in the copresence of 5% H_2O + 100 ppm SO_2 in the feed gas. The enhanced redox performance and NH_3 adsorption capacity of the $Mn_6Ce_{0.3}In_{0.7}O_x$ catalyst are related to the increase in the specific surface area of the catalyst and the increase in the ratio of Mn^{4+} ions and surface oxygen (O_α) on the surface.

https://doi.org/10.1021/acsomega.1c07000
ACS Omega 2022, 7, 6381−6392

4. EXPERIMENTAL SECTION

4.1. Catalysis Preparation. All samples were synthesized by coprecipitation. First, the $MnCeO_x$ catalyst was synthesized, in which Mn:Ce = 6:1 (molar ratio). Next, a series of $MnCeInO_x$ catalysts were prepared, in which Mn:(Ce + In) = 6:1 and Ce:In = 9:1, 7:3, 5:5, 3:7, and 1:9 (molar ratio). First, $Mn(CH_3COO)_2{\cdot}4H_2O$, $In(NO_3)_3{\cdot}H_2O$, and $Ce(NO_3)_3{\cdot}H_2O$ were added one by one to 100 mL of distilled water at a water bath at 30 °C and stirred until a clear solution. An equal stoichiometric ratio of $(NH_3)_2CO_3$ was dispersed in 10 mL of deionized water. It was then added into the clear salt solution. After continuous vigorous stirring, the mixture was adjusted to a pH value between 9 and 10 using 4 M NaOH solution and then covered with a cling film to be sealed, and the mixture was continued to be stirred for 2 h. Then, the suspension was allowed to stand at around 24 h at room temperature. The sediment was washed to pH = 7 using deionized water; then, the solid obtained was dried in a blast drying oven at 110 °C for 6 h. Finally, it was placed in a resistance furnace under an air atmosphere at 400 °C for 4 h. The prepared catalysts were named as $Mn_6Ce_{(a)}In_{(b)}O_x$ ($a + b = 1$). Mn_6CeO_x was prepared by a similar approach without the inclusion of indium.

4.2. Catalyst Characterization and Computational Details. X-ray diffractometry (XRD) analysis for the samples was performed using a SmartLab (9 kW) rotating-target X-ray diffractometer of Keshikoshi Corporation (Japan).

In the Brunauer−Emmett−Teller (BET) test, the samples were pretreated by degassing at 180 °C and 5 mTorr under vacuum at a steady state. They were then tested at −196 °C using a Quantachrome Instruments Quadrasorb EVO. The catalyst morphology was observed by field emission scanning electron microscopy (FE-SEM) on a 15 kV Merlin compact device made by Carl Zeiss NTS GmbH (Germany).

The X-ray photoelectron spectra (XPS) of the samples were documented on a Thermo Fisher ESCALAB 250Xi spectrometer using monochromatic Al Kα as the X-ray source, calibrated with the C 1s peak of indeterminate carbon (binding energy of 284.8 eV). The splitting calculations of the Mn 2p peak, O 1s peak, Ce 3d peak, and In 3d peak were performed using XPSPEAK 4.1 splitting software for inverse folded products, with Shirley as the background and the convolution Gaussian/Lorentzian ratio set to 80/20.

Temperature-programmed desorption (NH_3-TPD) of adsorbed NH_3 on the catalyst was carried out on an AUTO Chem II 2920 device (American Microelectronics Instruments, Inc.) equipped with a thermal conductivity detector (TCD). A 0.12 g sample was loaded into a quartz TPD reactor and pretreated in a 50 mL/min stream of N_2 and at 400 °C for 1 h. After waiting for the sample to cool to 50 °C, it was then purged with 10% NH_3/N_2 at a flow rate of 50 mL/min for 1 h to ensure complete saturation of the adsorption sites. The catalyst was then flushed with N_2 at the same gas flux for 1 h to take out the weakly sorbed NH_3. Then, the catalyst was heated from 50 to 800 °C with a constant N_2 flow rate with a ramp rate of 10 °C/min for NH_3 desorption, and the change in the NH_3 content during the process was detected in real time using a TCD detector.

Hydrogen temperature-programmed reduction (H_2-TPR) studies of mixed oxides were performed on an AUTO Chem II 2920 apparatus (American Microelectronics Instruments, Inc.) to determine their redox behavior. To perform these studies, a 0.12 g sample of the catalyst was put in a quartz U-shaped reaction cell. After the same sample pretreatment in pure argon as for NH_3-TPD studies, they were cooled to 50 °C in a stream of argon. The TCD signals were recorded in the temperature range of 50−800 °C with a 5% H_2/Ar mixture gas stream at a flow rate of 30 mL/min and a heating rate of 10 °C/min.

The surface adsorption of the catalyst was investigated by FTIR (Thermo Fisher) after the NH_3-SCR reaction and water and sulfur resistance tests.

4.3. Catalytic Performance Test. The schematic diagram of experimental equipment is shown in Figure 10. The catalytic activity of Mn_6CeO_x and $Mn_6Ce_{(a)}In_{(b)}O_x$ ($a + b = 1$) for NH_3-SCR in excess oxygen was studied in a vertical tubular furnace with a high-temperature-resistant quartz glass tube of 6 mm inner diameter, and the catalyst was placed in the heating section of the tubular furnace. Catalysts (40−60 mesh) (0.2 g) with a volume of about 0.25 mL were used. The reaction gas consists of 500 ppm NO, 500 ppm NH_3, 5% O_2, 100 ppm SO_2 (if used), 5% H_2O (if used), and balance N_2. The space velocity (GHSV) was about 120,000 h^{-1}. The concentration of NO_x was measured by an electrochemical gas analyzer (Cairn-May Quintox Flue Gas Analyzer). The NO_x conversion and N_2 selectivity were calculated using eqs 1 and 2, respectively:[20]

$$\begin{aligned} &NO_X \text{ conversion}(\%) \\ &= (1 - [NO_X]_{out}/[NO_X]_{in}) \times 100\%(NO_x \\ &= NO + NO_2) \end{aligned} \tag{1}$$

$$\begin{aligned} &N_2 \text{ selectivity}(\%) \\ &= \left(1 - \frac{2[N_2O]_{out} + [NO_2]_{out} - 2[N_2O]_{in} - [NO_2]_{in}}{[NH_3]_{in} + [NO_X]_{in} - [NH_3]_{out} - [NO_X]_{out}}\right) \\ &\times 100\% \end{aligned} \tag{2}$$

The corner mark in represents the concentration of a substance in the raw gas. The corner mark out represents the concentration of a substance after catalyst treatment.

Turnover frequency (TOF) values were calculated according to the following equation:[21]

$$TOF = \frac{\nu \times \alpha}{V_m \times n_a} \tag{3}$$

where ν is the flow rate of nitrogen oxide ($m^3{\cdot}s^{-1}$); α is the conversion of nitrogen oxide (%); V_m is the gas molar volume ($m^3{\cdot}mol^{-1}$); n_a is the number of moles of surface acidic sites (mol). The TOF values based on the surface acidic sites were estimated by NH_3-TPD.

The SCR kinetic parameters were calculated by the following equation:

$$k = -\frac{F}{W}\ln(1 - x) \tag{4}$$

where k is the reaction rate constant ($cm^3{\cdot}g^{-1}{\cdot}s^{-1}$), F is the total flow rate ($cm^3{\cdot}s^{-1}$), W is the mass of the catalyst (g), and x is the NO_x conversion.

Furthermore, the apparent activation energies (E_a) was calculated using the Arrhenius equation shown as follows:

$$k = Ae^{-E_a/RT} \tag{5}$$

https://doi.org/10.1021/acsomega.1c07000
ACS Omega 2022, 7, 6381−6392

AUTHOR INFORMATION

Corresponding Author

Haixia Li − *School of Mechanical and Power Engineering, Henan Polytechnic University, Jiaozuo 454000, China;* orcid.org/0000-0001-6665-809X; Email: lihx@hpu.edu.cn

Authors

Changze Yang − *School of Mechanical and Power Engineering, Henan Polytechnic University, Jiaozuo 454000, China*

Anchao Zhang − *School of Mechanical and Power Engineering, Henan Polytechnic University, Jiaozuo 454000, China;* orcid.org/0000-0002-0704-6736

Zhijun Sun − *School of Mechanical and Power Engineering, Henan Polytechnic University, Jiaozuo 454000, China*

Xinmin Zhang − *School of Mechanical and Power Engineering, Henan Polytechnic University, Jiaozuo 454000, China*

Shuaibo Zhang − *School of Mechanical and Power Engineering, Henan Polytechnic University, Jiaozuo 454000, China*

Leying Jin − *School of Mechanical and Power Engineering, Henan Polytechnic University, Jiaozuo 454000, China*

Zhiheng Song − *School of Mechanical and Power Engineering, Henan Polytechnic University, Jiaozuo 454000, China*

Complete contact information is available at: https://pubs.acs.org/10.1021/acsomega.1c07000

Notes

The authors declare no competing financial interest.

ACKNOWLEDGMENTS

This work was supported by the National Natural Science Foundation of China (U1504217, 51676064, and 51306046) and the Innovative Research Team of Henan Polytechnic University (T2020-3).

REFERENCES

(1) Zhao, B.; Wang, S. X.; Liu, H.; Xu, J. Y.; Fu, K.; Klimont, Z.; Hao, J. M.; He, K. B.; Cofala, J.; Amann, M. NO_x emissions in China: Historical trends and future perspectives. *Atmos. Chem. Phys.* **2013**, *13*, 9869−9897.

(2) Granger, P.; Parvulescu, V. I. Catalytic NO(x) abatement systems for mobile sources: from three-way to lean burn after-treatment technologies. *Chem. Rev.* **2011**, *111*, 3155−3207.

(3) Dahlin, S.; Englund, J.; Malm, H.; Feigel, M.; Westerberg, B.; Regali, F.; Skoglundh, M.; Pettersson, L. J. Effect of biofuel- and lube oil-originated sulfur and phosphorus on the performance of Cu-SSZ-13 and V_2O_5-WO_3/TiO_2 SCR catalysts. *Catal. Today* **2021**, *360*, 326−339.

(4) Zamansky, V. M.; Lissianski, V. V.; Maly, P. M.; Ho, L.; Rusli, D.; Gardiner, W. C., Jr. Reactions of sodium species in the promoted SNCR process. *Combust. Flame* **1999**, *117*, 821−831.

(5) Niu, Q.; Luo, J. J.; Zheng, J. S.; Wang, W.; Wang, K. T. Experimental Research for the Simultaneous Removal of NO and SO_2 in Flue Gas. *Guangdong Chem. Ind.* **2020**, *47*, 159−161.

(6) Zhang, H.; Kong, M.; Cai, Z.; Jiang, L.; Liu, Q.; Yang, J.; Ren, S.; Li, J.; Duan, M. Synergistic effect of arsenic and different potassium species on V_2O_5-WO_3/TiO_2 catalyst poisoning: Comparison of Cl^-, SO_4^{2-} and NO^{3-} anions. *Catal. Commun.* **2020**, *144*, 106069.

(7) Putluru, S. S. R.; Schill, L.; Godiksen, A.; Poreddy, R.; Mossin, S.; Jensen, A. D.; Fehrmann, R. Promoted V_2O_5/TiO_2 catalysts for selective catalytic reduction of NO with NH_3 at low temperatures. *Appl. Catal. B* **2016**, *183*, 282−290.

(8) Thiyagu, S.; Naveen, T. K.; Siddharthan, B.; Manirathnam, A. S. Numerical investigation and performance enhancement of 210 MW boiler by utilization of waste heat in flue gas. *Mater. Today* **2020**, *33*, 756−762.

(9) Han, Y.; Sun, Y. Y. Collaborative optimization of energy conversion and NO_x removal in boiler cold-end of coal-fired power plants based on waste heat recovery of flue gas and sensible heat utilization of extraction steam. *Energy* **2020**, *207*, 118172.

(10) Topsoe, N. Y. Mechanism of the selective catalytic reduction of nitric oxide by ammonia elucidated by in situ on-line fourier transform infrared spectroscopy. *Science* **1994**, *265*, 1217−1219.

(11) Peng, Y.; Chang, H.; Dai, Y.; Li, J. Structural and Surface Effect of MnO_2 for Low Temperature Selective Catalytic Reduction of NO with NH_3. *Procedia Environ. Sci.* **2013**, *18*, 384−390.

(12) Yang, C.; Yang, J.; Jiao, Q.; Zhao, D.; Zhang, Y.; Liu, L.; Hu, G.; Li, J. Promotion effect and mechanism of MnO_x doped CeO_2 nano-catalyst for NH_3-SCR. *Ceram. Int.* **2020**, *46*, 4394−4401.

(13) Li, L.; Sun, B.; Sun, J.; Yu, S.; Ge, C.; Tang, C.; Dong, L. Novel MnO_x-CeO_2 nanosphere catalyst for low-temperature NH_3-SCR. *Catal. Commun.* **2017**, *100*, 98−102.

(14) Andreoli, S.; Deorsola, F. A.; Pirone, R. MnO_x-CeO_2 catalysts synthesized by solution combustion synthesis for the low-temperature NH_3-SCR. *Catal. Today* **2015**, *253*, 199−206.

(15) Qi, G.; Yang, R. T.; Chang, R. MnO_x-CeO_2 mixed oxides prepared by co-precipitation for selective catalytic reduction of NO with NH_3 at low temperatures. *Appl. Catal. B* **2004**, *51*, 93−106.

(16) Qi, G.; Yang, R. T. Performance and kinetics study for low-temperature SCR of NO with NH_3 over MnO_x-CeO_2 catalyst. *J. Catal.* **2003**, *217*, 434−441.

(17) Liu, Q.; Fu, Z.; Ma, L.; Niu, H.; Liu, C.; Li, J.; Zhang, Z. MnO_x-CeO_2 supported on Cu-SSZ-13: A novel SCR catalyst in a wide temperature range. *Appl. Catal., A* **2017**, *547*, 146−154.

(18) Decolatti, H. P.; Martínez-Hernández, A.; Gutiérrez, L. B.; Fuentes, G. A.; Zamaro, J. M. Characterization of dispersed indium species obtained by thermal treatment of In-NH_4-zeolites and their impact on the SCR of NO_x. *Microporous Mesoporous Mater.* **2011**, *145*, 41−50.

(19) Pan, H.; Jian, Y.; Yu, Y.; He, C.; Shen, Z.; Liu, H. Regeneration and sulfur poisoning behavior of In/H-BEA catalyst for NO_x reduction by CH_4. *Appl. Surf. Sci.* **2017**, *401*, 120−126.

(20) Tan, H.; Ma, S.; Zhao, X.; Li, Y.; Zhao, C.; Zhu, Y. Excellent low-temperature NH_3-SCR of NO activity and resistance to H_2O and SO_2 over W_aCeO_x (a=0.06, 0.12, 0.18, 0.24) catalysts: Key role of acidity derived from tungsten addition. *Appl. Catal., A* **2021**, *627*, 118374.

(21) Wu, X.; Meng, H.; Du, Y.; Liu, J.; Hou, B.; Xie, X. Insight into Cu_2O/CuO collaboration in the selective catalytic reduction of NO with NH_3: Enhanced activity and synergistic mechanism. *J. Catal.* **2020**, *384*, 72−87.

(22) Jin, R.; Liu, Y.; Wu, Z.; Wang, H.; Gu, T. Relationship between SO_2 poisoning effects and reaction temperature for selective catalytic reduction of NO over Mn-Ce/TiO_2 catalyst. *Catal. Today* **2010**, *153*, 84−89.

(23) Yan, D. J.; Guo, T.; Yu, Y.; Chen, Z. H. Lead poisoning and regeneration of Mn-Ce/TiO_2 catalysts for NH_3-SCR of NO at low temperature. *J. Fuel Chem. Technol.* **2021**, *49*, 113−120.

(24) Wang, H.; Jia, J.; Liu, S.; Chen, H.; Wei, Y.; Wang, Z.; Zheng, L.; Wang, Z.; Zhang, R. Highly Efficient NO Abatement over Cu-ZSM-5 with Special Nanosheet Features. *Environ. Sci. Technol.* **2021**, *55*, 5422−5434.

(25) Liu, Z.; Chen, C.; Zhao, J.; Yang, L.; Sun, K.; Zeng, L.; Pan, Y.; Liu, Y.; Liu, C. Study on the NO_2 production pathways and the role of NO_2 in fast selective catalytic reduction DeNO$_x$ at low-temperature over MnO_x/TiO_2 catalyst. *Chem. Eng. J.* **2020**, 379.

(26) Wu, X. M.; Ni, K. W.; Yu, X. L.; Zhao, N. In-situ DRIFTs study on different exposed facets of VO_x-MnO_x/CeO_2 catalysts for low-temperature NH_3-SCR. *J. Fuel Chem. Technol.* **2020**, *48*, 179−188.

(27) Wu, H.; He, M.; Liu, W.; Jiang, L.; Cao, J.; Yang, C.; Yang, J.; Peng, J.; Liu, Y.; Liu, Q. Application of manganese-containing soil as

novel catalyst for low-temperature NH_3-SCR of NO. *J. Environ. Chem. Eng.* **2021**, *9*, 105426.
(28) Jiang, B.; Li, Z.; Lee, S.-c. Mechanism study of the promotional effect of O_2 on low-temperature SCR reaction on Fe-Mn/TiO_2 by DRIFT. *Chem. Eng. J.* **2013**, *225*, 52−58.
(29) Gao, F.; Tang, X.; Yi, H.; Li, J.; Zhao, S.; Wang, J.; Chu, C.; Li, C. Promotional mechanisms of activity and SO_2 tolerance of Co- or Ni-doped MnOx-CeO_2 catalysts for SCR of NOx with NH_3 at low temperature. *Chem. Eng. J.* **2017**, *317*, 20−31.
(30) Yu, Y.; Tan, W.; An, D.; Wang, X.; Liu, A.; Zou, W.; Tang, C.; Ge, C.; Tong, Q.; Sun, J.; Dong, L. Insight into the SO_2 resistance mechanism on γ-Fe_2O_3 catalyst in NH_3-SCR reaction: A collaborated experimental and DFT study. *Appl. Catal. B* **2021**, *281*, 119544.
(31) Liu, Y. Z.; Guo, R. T.; Duan, C. P.; Wu, G. L.; Miao, Y. F.; Gu, J. W.; Pan, W. G. A highly effective urchin-like $MnCrO_x$ catalyst for the selective catalytic reduction of NO_x with NH_3. *Fuel* **2020**, *271*, 117667.
(32) Kang, H.; Wang, J.; Zheng, J.; Chu, W.; Tang, C.; Jiawei, J.; Ren, R.; Wu, M.; Jing, F. Solvent-free elaboration of Ni-doped MnO_x catalysts with high performance for NH_3-SCR in low and medium temperature zones. *Mol. Catal.* **2021**, *501*, 111376.
(33) Wang, C.; Yu, F.; Zhu, M.; Tang, C.; Zhang, K.; Zhao, D.; Dong, L.; Dai, B. Highly selective catalytic reduction of NO_x by MnO_x-CeO_2-Al_2O_3 catalysts prepared by self-propagating high-temperature synthesis. *J. Environ. Sci.* **2019**, *75*, 124−135.
(34) Huang, X.; Dong, F.; Zhang, G.; Guo, Y.; Tang, Z. A strategy for constructing highly efficient yolk-shell Ce@Mn@TiO_x catalyst with dual active sites for low-temperature selective catalytic reduction of NO with NH_3. *Chem. Eng. J.* **2021**, *419*, 129572.
(35) Fang, N.; Guo, J.; Shu, S.; Luo, H.; Chu, Y.; Li, J. Enhancement of low-temperature activity and sulfur resistance of $Fe_{0.3}Mn_{0.5}Zr_{0.2}$ catalyst for NO removal by NH_3-SCR. *Chem. Eng. J.* **2017**, *325*, 114−123.
(36) Wang, R.; Hao, Z.; Li, Y.; Liu, G.; Zhang, H.; Wang, H.; Xia, Y.; Zhan, S. Relationship between structure and performance of a novel highly dispersed MnO_x on Co-Al layered double oxide for low temperature NH_3-SCR. *Appl. Catal. B* **2019**, *258*, 117983.
(37) Xu, Q.; Fang, Z.; Chen, Y.; Guo, Y.; Guo, Y.; Wang, L.; Wang, Y.; Zhang, J.; Zhan, W. Titania-Samarium-Manganese Composite Oxide for the Low-Temperature Selective Catalytic Reduction of NO with NH_3. *Environ. Sci. Technol.* **2020**, *54*, 2530−2538.
(38) Chang, H.; Li, J.; Yuan, J.; Chen, L.; Dai, Y.; Arandiyan, H.; Xu, J.; Hao, J. Ge, Mn-doped CeO_2−WO_3 catalysts for NH_3−SCR of NO_x: Effects of SO_2 and H_2 regeneration. *Catal. Today* **2013**, *201*, 139−144.
(39) Meng, D.; Xu, Q.; Jiao, Y.; Guo, Y.; Guo, Y.; Wang, L.; Lu, G.; Zhan, W. Spinel structured $Co_aMn_bO_x$ mixed oxide catalyst for the selective catalytic reduction of NO_x with NH_3. *Appl. Catal. B* **2018**, *221*, 652−663.
(40) Gu, T.; Liu, Y.; Weng, X.; Wang, H.; Wu, Z. The enhanced performance of ceria with surface sulfation for selective catalytic reduction of NO by NH_3. *Catal. Commun.* **2010**, *12*, 310−313.
(41) Ali, S.; Chen, L.; Li, Z.; Zhang, T.; Li, R.; Bakhtiar, S. u. H.; Leng, X. Cu_X-$Nb_{1.1-X}$ (x = 0.45, 0.35, 0.25, 0.15) bimetal oxides catalysts for the low temperature selective catalytic reduction of NO with NH_3. *Appl. Catal.B* **2018**, *236*, 25−35.
(42) Fan, Z.; Shi, J.-W.; Gao, C.; Gao, G.; Wang, B.; Wang, Y.; He, C.; Niu, C. Gd-modified MnO_x for the selective catalytic reduction of NO by NH_3: The promoting effect of Gd on the catalytic performance and sulfur resistance. *Chem. Eng. J.* **2018**, *348*, 820−830.
(43) Shen, B.; Wang, F.; Liu, T. Homogeneous MnO-CeO_2 pellets prepared by a one-step hydrolysis process for low-temperature NH_3-SCR. *Powder Technol.* **2014**, *253*, 152−157.
(44) Wang, J. H.; Cui, H. L.; Dong, X. S.; Zhao, H. W.; Wang, Y. J.; Chen, H.; Yao, M. F.; Li, Y. D. N_2O formation in the selective catalytic reduction of NO_x with NH_3 on a $CeMoO_x$ catalyst. *Appl. Catal. A: Gen.* **2015**, *505*, 8−15.
(45) Naik, M. Z.; Salker, A. V. Effect of indium doping on magnetic properties of cerium oxide nanoparticles. *Mater. Chem. Phys.* **2018**, *212*, 336−342.
(46) Li, H.; Wu, C.-Y.; Li, Y.; Zhang, J. Superior activity of MnO_x-CeO_2/TiO_2 catalyst for catalytic oxidation of elemental mercury at low flue gas temperatures. *Appl. Catal. B* **2012**, *111-112*, 381−388.
(47) Liu, Z.; Zhu, J.; Li, J.; Ma, L.; Woo, S. I. Novel Mn-Ce-Ti mixed-oxide catalyst for the selective catalytic reduction of NO_x with NH_3. *ACS Appl. Mater. Interfaces* **2014**, *6*, 14500−14508.
(48) Zamaro, J. M.; Miró, E. E.; Boix, A. V.; Martínez-Hernández, A.; Fuentes, G. A. In−zeolites prepared by oxidative solid state ion exchange (OSSIE): Surface species and structural characterization. *Microporous Mesoporous Mater.* **2010**, *129*, 74−81.
(49) Pan, H.; Jian, Y. F.; Yu, Y. K.; Chen, N. N.; He, C.; He, C. Promotional mechanism of propane on selective catalytic reduction of NO_x by methane over In/H-BEA at low temperature. *Appl. Surf. Sci.* **2016**, *390*, 608−616.
(50) Li, X.; Cheng, J.; Gao, Y.; Li, M.; Kuang, D.; Li, Y.; Xue, J.; Zhang, T.; Yu, Z. Impact of NH_3 plasma treatment for solution-processed indium oxide thin-film transistors with low thermal budget. *J. Alloys Compd.* **2020**, *817*, 152720.
(51) Chen, S.; Vasiliades, M. A.; Yan, Q.; Yang, G.; Du, X.; Zhang, C.; Li, Y.; Zhu, T.; Wang, Q.; Efstathiou, A. M. Remarkable N_2-selectivity enhancement of practical NH_3-SCR over $Co_{0.5}Mn_1Fe_{0.25}Al_{0.75}O_x$-LDO: The role of Co investigated by transient kinetic and DFT mechanistic studies. *Appl. Catal. B* **2020**, *277*, 119186.
(52) Li, N.; Wang, A.; Liu, Z.; Wang, X.; Zheng, M.; Huang, Y.; Zhang, T. On the catalytic nature of Mn/sulfated zirconia for selective reduction of NO with methane. *Appl. Catal. B* **2006**, *62*, 292−298.
(53) Qu, Z.; Gao, K.; Fu, Q.; Qin, Y. Low-temperature catalytic oxidation of toluene over nanocrystal-like Mn-Co oxides prepared by two-step hydrothermal method. *Catal. Commun.* **2014**, *52*, 31−35.
(54) Chen, L.; Yao, X.; Cao, J.; Yang, F.; Tang, C.; Dong, L. Effect of Ti^{4+} and Sn^{4+} co-incorporation on the catalytic performance of CeO_2-MnO_x catalyst for low temperature NH_3-SCR. *Appl. Surf. Sci.* **2019**, *476*, 283−292.
(55) Peng, Y.; Li, J.; Huang, X.; Li, X.; Su, W.; Sun, X.; Wang, D.; Hao, J. Deactivation Mechanism of Potassium on the V_2O_5/CeO_2 Catalysts for SCR Reaction: Acidity, Reducibility and Adsorbed-NO_x. *Environ. Sci. Technol.* **2014**, *48*, 4515−4520.
(56) Berndt, H.; Schutze, F.-W.; Richter, M.; Sowade, T.; Grünert, W. Selective catalytic reduction of NO under lean conditions by methane and propane over indium/cerium-promoted zeolites. *Appl. Catal. B* **2003**, *40*, 51−67.
(57) Zhang, Z.; Li, R.; Wang, M.; Li, Y.; Tong, Y.; Yang, P.; Zhu, Y. Two steps synthesis of $CeTiO_x$ oxides nanotube catalyst: Enhanced activity, resistance of SO_2 and H_2O for low temperature NH_3-SCR of NO_x. *Appl. Catal. B* **2021**, *282*, 119542.
(58) Shi, Y.; Yi, H.; Gao, F.; Zhao, S.; Xie, Z.; Tang, X. Evolution mechanism of transition metal in NH_3-SCR reaction over Mn-based bimetallic oxide catalysts: Structure-activity relationships. *J. Hazard. Mater.* **2021**, *413*, 125361.
(59) Song, D.; Shao, X.; Yuan, M.; Wang, L.; Zhan, W.; Guo, Y.; Guo, Y.; Lu, G. Selective catalytic oxidation of ammonia over MnO_x-TiO_2 mixed oxides. *RSC Adv.* **2016**, *6*, 88117−88125.
(60) Ji, J.; Jing, M.; Wang, X.; Tan, W.; Guo, K.; Li, L.; Wang, X.; Song, W.; Cheng, L.; Sun, J.; Song, W.; Tang, C.; Liu, J.; Dong, L. Activating low-temperature NH_3-SCR catalyst by breaking the strong interface between acid and redox sites, A case of model $Ce_2(SO_4)_3$-CeO_2 study. *J. Catal.* **2021**, *399*, 212−223.
(61) Xue, H.; Guo, X.; Meng, T.; Mao, D.; Ma, Z. NH_3-SCR of NO over M/ZSM-5 (M = Mn, Co, Cu) catalysts: An in-situ DRIFTS study. *Surfaces and Interfaces* **2022**, *29*, 101722.
(62) Chen, L.; Ren, S.; Liu, L.; Su, B.; Yang, J.; Chen, Z.; Wang, M.; Liu, Q. Catalytic performance over Mn-Ce catalysts for NH_3-SCR of NO at low temperature: Different zeolite supports. *J. Environ. Chem. Eng.* **2022**, *10*, 107167.

https://doi.org/10.1021/acsomega.1c07000
ACS Omega 2022, 7, 6381−6392

(63) Pu, Y.; Yang, L.; Yao, C.; Jiang, W.; Yao, L. Low-cost Mn-Fe/SAPO-34 catalyst from natural ferromanganese ore and lithium-silicon-powder waste for efficient low-temperature NH_3-SCR removal of NO_x. *Chemosphere* **2022**, *293*, 133465.

https://doi.org/10.1021/acsomega.1c07000
ACS Omega 2022, 7, 6381−6392